PERIODICO di MINERALOGIA
established in 1930

DIPARTIMENTO
DI SCIENZE DELLA TERRA

SAPIENZA
UNIVERSITÀ DI ROMA

An International Journal of
Mineralogy, Crystallography, Geochemistry,
Ore Deposits, Petrology, Volcanology
and applied topics on Environment, Archaeometry and Cultural Heritage

Nature of tourmaline formation in quartz porphyry in the E Sakarya zone (NE Turkey): geochemistry and isotopic approach

Ferkan Sipahi *

Department of Geology Engineering, Gümüşhane University, 29000, Gümüşhane, Turkey

ARTICLE INFO

Submitted: March 2019
Accepted: July 2019
Available on line: July 2019

* Corresponding author:
ferkansipahi@gmail.com

DOI: 10.2451/2019PM859

How to cite this article:
Sipahi F. (2019)
Period. Mineral. 88, 333-351

ABSTRACT

Tourmaline, which exhibits important differences in terms of texture and composition, is found in 44 My aged quartz porphyry from Karadağ in the eastern Pontide (NE Turkey). Tourmaline has high Al and Mg contents and is the chemical zoning; it contains Mg that can substitute for Fe and/or Al in the Y site and X-vacancy that can replace Na in the X site from the core to rim. Tourmaline, classified as dravite component, has low Fe content and very low Ca content. The V (112-510 ppm) and Sr (37.3-147.1 ppm) contents of tourmalines related to quartz porphyry are in conformity with metamorphic and magmatic tourmalines. Tourmalines have similar rare earth elements (REEs) but lower heavy REE contents than host quartz porphyry. The $\delta^{18}O$ and δD values of tourmalines are relatively narrow, ranging from 5.7 to 8.5‰ V-SMOW and from -58 to -72‰ V-SMOW, respectively, consistent with primary magmatic water. The oxygen-isotope thermometry calculation of quartz and tourmaline pair yields equilibrium formation temperature of 432 °C. The formation of tourmaline shows a post magmatic origin, confirming magmatic fluid cooling and fluid-rock interactions.

Keywords: Geochemistry; O- and H- isotopes; quartz porphyry; tourmaline; Eastern Pontide; Turkey.

INTRODUCTION

Tourmaline in granitic, sedimentary, and metamorphic rocks is an important mineral used as indicator of petrogenetic nature and mineral deposits (Henry and Guidotti, 1985; Slack, 1996; Oyman, 2006; Yavuz et al., 2008, 2011; Koralay et al., 2013; Yücel-Öztürk et al., 2015). Tourmaline can be found in different geological environments, such as volcanogenic massive sulfide mineralization, sedimentary-exhalative Zn-Pb-Ag mineralization, Cu-Au breccia pipes, porphyr-type Cu-Mo mineralization, and Sn-W vein in or near granite (Slack et al., 1993; Jiang et al., 1995; Deb et al., 1997; Lynch and Ortega, 1997; Skewes et al., 2003; Mlynarczyk and Williams-Jones, 2006; Neiva et al., 2007). The geochemical and isotopic characteristics of tourmalines in Turkey and around the world were described by some researchers (Table 1). Tourmaline can have various major and trace elements. Thus, the chemistry and isotopic composition of tourmaline provides information about the origin of tourmaline and its host rocks (Palmer, 1991; Pirajno and Smithies, 1992; Jiang et al., 1998). Tourmaline has high Sr content but low Rb content (King and Kerrich, 1989; Griffin et al., 1996; Jiang et al., 1997). The rare earth element content of tourmaline in various rocks and ore minerals is a good index of petrogenesis and ore genesis (Jolliff et al., 1987; King et al., 1988; Hellingwerf et al., 1994; Jiang and Palmer, 1995; Jiang et al., 1997). Together with the major, trace, and rare earth element compositions and the stable isotope chemistry of tourmaline, this work provides new insights into the source of tourmaline. Moreover, tourmaline can be used to understand the geological history of geodynamic evolution of the E Sakarya Zone.

Table 1. The geochemical and isotopic data of tourmaline occurrences in Turkey and the World.

Location	Host Rock	Tourmaline composition	Some trace element values (V and Sr)	Isotopic composition ($\delta^{18}O$ and δD)	Genesis	References
Sinancılar-Kemalpaşa, W Turkey	Granit, aplit, pegmatite	Dravite, schorl	-	-	The contact metamorphic processes after regional metamorphism and the following hydrothermal activities	Oyman (2006)
Şebinkarahisar NE Turkey	Asarcık granitoid and quartz veins	Schorl-dravite	V (47-143 ppm) Sr (79-430 ppm)	-	Magmatic-hydrothermal evolution	Yavuz et al. (2011)
Buldan, Denizli, W Turkey	Pegmatite	Schorl	V (245-591.4 ppm) Sr (152.9-212.4 ppm)	-	Probably generated from Li-poor granitoid and their associated pegmatite	Koralay et al. (2013)
Western Anatolia, Turkey	Menderes Massif	Dravite-schorl	-	-	Metasomatism of the lithospheric mantle beneath the Menderes massif	Yücel-Öztürk et al. (2015)
Broken Hill District, Australia	Tourmaline-rich rocks	Schorl-dravite	V (15-189 ppm) Sr (23-225 ppm)	-	Submarine hydrothermal process	Slack et al. (1993)
Dachang Sn-polymetallic ore deposit, China	Siliceous rocks and quartz-tourmaline veins in or near the granite	Dravite-schorl	V (54-2056 ppm) Sr (8.8-391 ppm)	-	A submarine exhalative-hydrothermal origin	Jiang et al. (1999)
São Paulo, Brazil	Iron formation and quartz veins	Schorl-dravite	V (138-488 ppm) Sr (444-497 ppm)	$\delta^{18}O$ (11.5 to 13.5‰ VSMOW) δD (-86 to -104‰ VSMOW)	Under submarine, sedimentary-exhalative conditions	Garda et al. (2003)
W Carpathians	Tatra Granite	Schorl-dravite	-	-	Possibly boiling oxidized fluid, exsolved from the cooling granitoid magma	Gaweda et al. (2013)
Variscan Schwarzwald, Germany	Granitic pegmatite, migmatitic gneiss and hydrothermal vein	Dravite-schorl	V (1-425 ppm) Sr (0.1-696 ppm)	$\delta^{18}O$ (9.3 to 11‰ V-SMOW)	Complexity of granite-related hydrothermal system	Marks et al. (2013)
Cornubian, SW England	Batholith	Schorl, dravite, elbaite, uvite, feruvite, foitite and Mg-foitite	V (0.1-2720 ppm) Sr (0.8-799 ppm)	-	The process of late-magmatic fractional crystallization	Duchoslav et al. (2017)
Karadağ, NE Turkey	Q-porphyry	Dravite	V (112-510 ppm) Sr (37.3-147.1 ppm)	$\delta^{18}O$ (5.7 to 8.5‰ VSMOW) δD (-58 to -72‰ VSMOW)	A post magmatic origin	This study

In Turkey, tourmalines are mostly seen in Menderes massif in the western Anatolia and rarely in Şebinkarahisar and Karadağ in the eastern of the Sakarya Zone. The tourmaline source in the Karadağ area is located in the eastern of the Sakarya Zone and is hosted by quartz porphyry. Quartz porphyry has been studied to understand the mineralogical and petrographic properties and define tourmaline (Özdoğan, 1992). However, the importance of tourmaline as a petrogenetic indicator for mineral deposits has not been investigated yet. Tourmaline in the Karadağ area was first investigated here. The present study conducted microscopy, mineral chemistry, analysis of trace and earth elements, and O- and H-isotope data for tourmaline and the geochemistry of quartz porphyry from the Karadağ area (Torul, Gümüşhane) in the northeastern Black Sea (Pontide) Metallogenic Belt of Turkey and compared with those of tourmaline from Turkey and the world.

GEOLOGICAL BACKGROUND

The Eastern Pontide, called the eastern part of the Sakarya Zone, Orogenic Belt of Turkey, is located within the Alpine Metallogenic Belt, which was developed during Mesozoic and Cenozoic cycle stretches from the European Alps, through the Carpathians, Anatolia, Caucasus, Zagros, Alborz to the Himalayan. The Eastern Pontides Orogenic Belt, geologically a typical palaeo-island arc forming above the northern Tethys subduction zone, contains various rock types. The northern part of the belt is defined by the Late Mesozoic and Cenozoic igneous rocks and ore deposits (Sipahi, 2011; Kaygusuz et al., 2014; Akaryalı, 2016; Sipahi et al., 2017; Sipahi et al., 2018 a,b). Eastern Pontides is located above sea level probably due to the collision between the Pontide magmatic arc and the Tauride-Anatolide block from Paleocene to Early Eocene because of the closure of the Neotethys (Okay and Tüysüz, 1999; Boztuğ et al., 2004). The collision in the late Paleocene to early Eocene was proposed by Okay et al. (1997) based on field relationships and pluton ages. The early Eocene adakitic rock showing a syn- to post-collision phase has been reported in the region (Topuz et al., 2005). The Middle Eocene cycle contains a large belt of east-west trending volcanic and plutonic rocks (Yılmaz and Boztuğ, 1996; Boztuğ et al., 2004) toward Iran and the Caucasus.

The ore mineralizations of the Gümüşhane area in the Eastern Black Sea Region were investigated by some researchers (e.g., Sipahi and Sadıklar, 2010; Sipahi, 2011; Akaryalı, 2016; Sipahi et al., 2017; Sipahi et al., 2018b). However, studies on granitoids and tourmaline in Karadağ area are limited (only mineralogical and petrographic, no chemical investigations) and primarily focus on general geology.

The Karadağ area is settled within the northern part of the Eastern Pontide Orogenic Belt (Figure 1a). Country rocks around the quartz porphyry consist of Late Cretaceous basalt, andesite, and limestone (Figure 1b). Field observations show that quartz porphyry includes tourmaline (Figure 2). Quartz porphyry, which has medium granular texture, is composed of quartz, orthoclase, plagioclase with albite twin, secondary muscovite, and opaque minerals (Figure 3 a,b) as well as zircon as an accessory mineral.

PETROGRAPHY OF HOST ROCK

The quartz porphyry is light gray and has medium to coarse grains. The age of the quartz porphyry is 44.27±0.46 Ma from U-Pb zircon age and is composed of quartz, orthoclase, oligoclasic plagioclase with albite twin, secondary muscovite, and opaque minerals (Figure 3a-b). Zircon forms the accessory phases. The quartz porphyry has peraluminous (1.09-3.02) characteristic.

PETROGRAPHY OF TOURMALINE FORMATION

Tourmaline shows radial spotted texture in the quartz porphyry (Figure 2 a,b). Tourmaline occurs radially in the shear zone and among the breccias of the quartz porphyry in the Karadağ area (Figure 2 c,d). Tourmaline is black or greenish black in macroscopic images. Tourmaline grains have sizes of up to several centimeters. Tourmalines in the shear zone are 2 cm thick (Figure 2c). Tourmalines among the quartz porphyry breccias are black (Figure 2d).

Tourmalines from the quartz porphyry show different forms in thin section (Figure 3 c,d). In general, tourmaline exists in tabular and round forms. Round tourmalines cut the tabular tourmaline and have concentric zone with dark greenish brown cores surrounded by light greenish brown rims (Figure 3 c,e). Boundaries between the core and rim are generally irregular. Tourmalines also have bluish green color (Figure 3 d,f). Hematite, a supergene oxidation mineral, occurs as cement between tourmaline grains (Figure 2e).

ANALYTICAL METHOD

Six quartz porphyry and four tourmaline samples were obtained from commercial ACME Laboratories, Ltd. (Canada) for analyses of major, trace, and rare earth elements. Major elements were analyzed with inductively coupled plasma-atomic emission spectrometry after fusion with $LiBO_2$. The powder sample (0.2 g) and $LiBO_2$ flux (1.5 g) were mixed in a graphite crucible and heated to 1050 °C for 15 min for analyses of trace and rare earth elements. The detection limit was set within the range of 0.01 wt% to 0.1 wt% for major oxides, 0.1 ppm to 10 ppm for trace elements, and 0.01 ppm to 0.5 ppm for rare earth elements.

Zircon U-Th-Pb isotopes were analyzed using

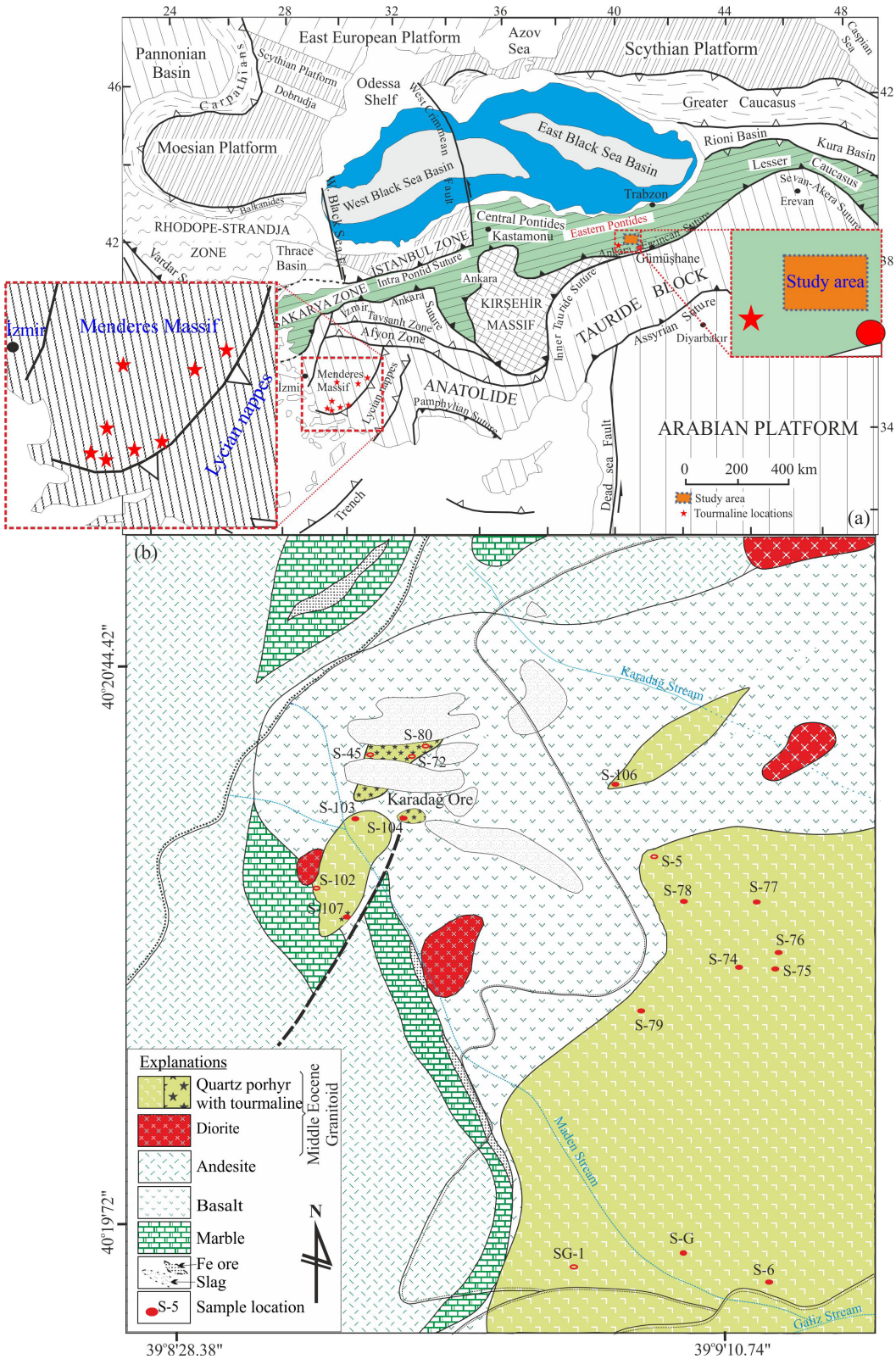

Figure 1. a) Regional tectonic setting of Turkey in relation to the Afro-Arabian and Eurasian plates (modified from Okay and Tüysüz, 1999) and b) A geological map of the investigated area (modified from Sipahi et al., 2017b). Tourmaline locations in the Figure 1a are from Koralay et al. (2013), Yücel et al. (2015) and Yavuz et al. (2008).

Figure 2. Tourmalines in the quartz porphyry. a) Radial tourmaline, b) Radial tourmaline spots, c) Tourmalines in the shear zone, and d) tourmaline among the breccias. Tur: Tourmaline.

SHRIMP IIe/MC at the Korea Basic Science Institute. A 2-4 nA mass filtered O_2^- primary beam was focused to the elliptical spot of ca. 20×25 µm diameter, with a 120 microns Kohler aperture, on the polished surface of zircon with 10 kV accelerating voltage. Each spot was rastered with the primary beam for 2-3 minutes before the analysis. Five cycles were conducted with a single electron multiplier. The collector slit was fixed at 100 µm in width to achieve mass resolution of about 5000 at 1% peak height. FC1 (1099 Ma; Paces and Miller, 1993) and SL13 (U=238 ppm) standard zircons were used for Pb/U calibration and U abundance, respectively. The Pb/U ratio was calibrated against FC1 by using its power law relationship between Pb^+/U^+ and UO^+/U^+, whereas the Th/U ratio was calculated using a fractionation factor derived from the measured $^{232}Th^{16}O^+/^{238}U^{16}O^+$ versus $^{208}Pb/^{206}Pb$ of the SL13 standard. Common Pb was removed by the ^{207}Pb (for dates <1000 Ma) or ^{204}Pb (for dates >1000 Ma) correction method by using the model of Stacey and Kramers (1975). Data processing was performed using SQUID 2.50 and Isoplot 3.75 programs running under Excel 2003 (Ludwig, 2008). Zircons with high U concentrations (>2500 ppm) were corrected using the algorithm established by Williams and Hergt (2000).

The electron microprobe analysis of tourmalines on carbon-coated polished section was conducted at the New Mexico Institute of Mining and Technology (USA) by using a Cameca SX-100 electron microprobe with three wavelength dispersive (WD) spectrometers. Microanalyses were carried out at an accelerating voltage (15 kV) and probe current (20 nA), with peak count times of 20 s for all elements, except for F (40 s; amph/mica), F (60 s; glass). Analyses of amp/mica was made using a point beam of 1 µm. Standard reference materials are Kaersutite (UCB), biotite (UCB), and magnetite (UCB).

Oxygen and hydrogen isotopes were measured at the Queen's Facility for Isotope Research (Canada). Tourmaline was analyzed for $\delta^{18}O$ and δD values, and quartz was evaluated for $\delta^{18}O$ value. The results were calibrated to certified reference materials declared in standard per mil notation (‰) and according to the international standards (VSMOW for $\delta^{18}O$, VSMOW for δ^2H). The primary or secondary standard analyses indicated the accuracy reported (1.5‰ for δ^2H, 0.5‰ for $\delta^{18}O$) per mil notation (‰).

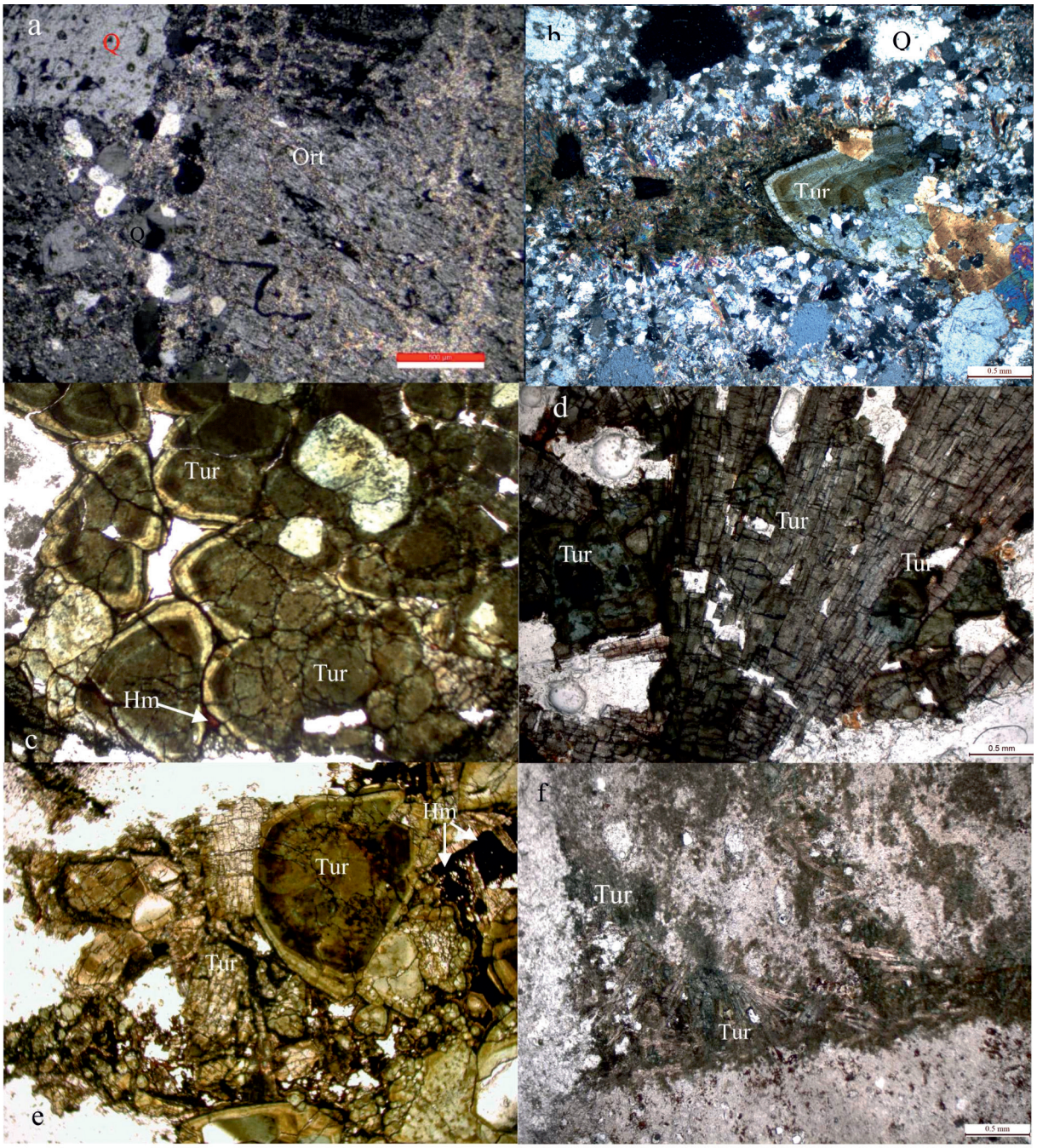

Figure 3. Thin sections of quartz porphyry and tourmaline from Karadağ. a) and b) Quartz porphyr (Sample no: SG-1, +N), c) Round and concentric zoned tourmaline (Sample no: S-71T, //N), d) Radial tourmaline (Sample no: S-71T, //N), e) Radial tourmalines among breccias (Sample no: S-80T, //N) and f) Tourmalines in the shear zone (Sample no: S-80T, //N). Q: Quartz, Ort: Orthoclase, Tur: Tourmaline, Hm: Hematite.

RESULTS

SHRIMP U-Pb zircon dating of the host rock

Knowledge on the emplacement age of the quartz porphyry from Karadağ is unsatisfactory because of contact relationships and stratigraphic criterion; a Late Cretaceous age was guessed by Özdoğan (1992). Table S1 presents the SHRIMP U-Pb zircon dating results of the quartz porphyry. The analyzed zircon grains are colorless, euhedral, and short to long prismatic in appearance (Figure 4a). The zircon grains are usually fine (i.e., 30-

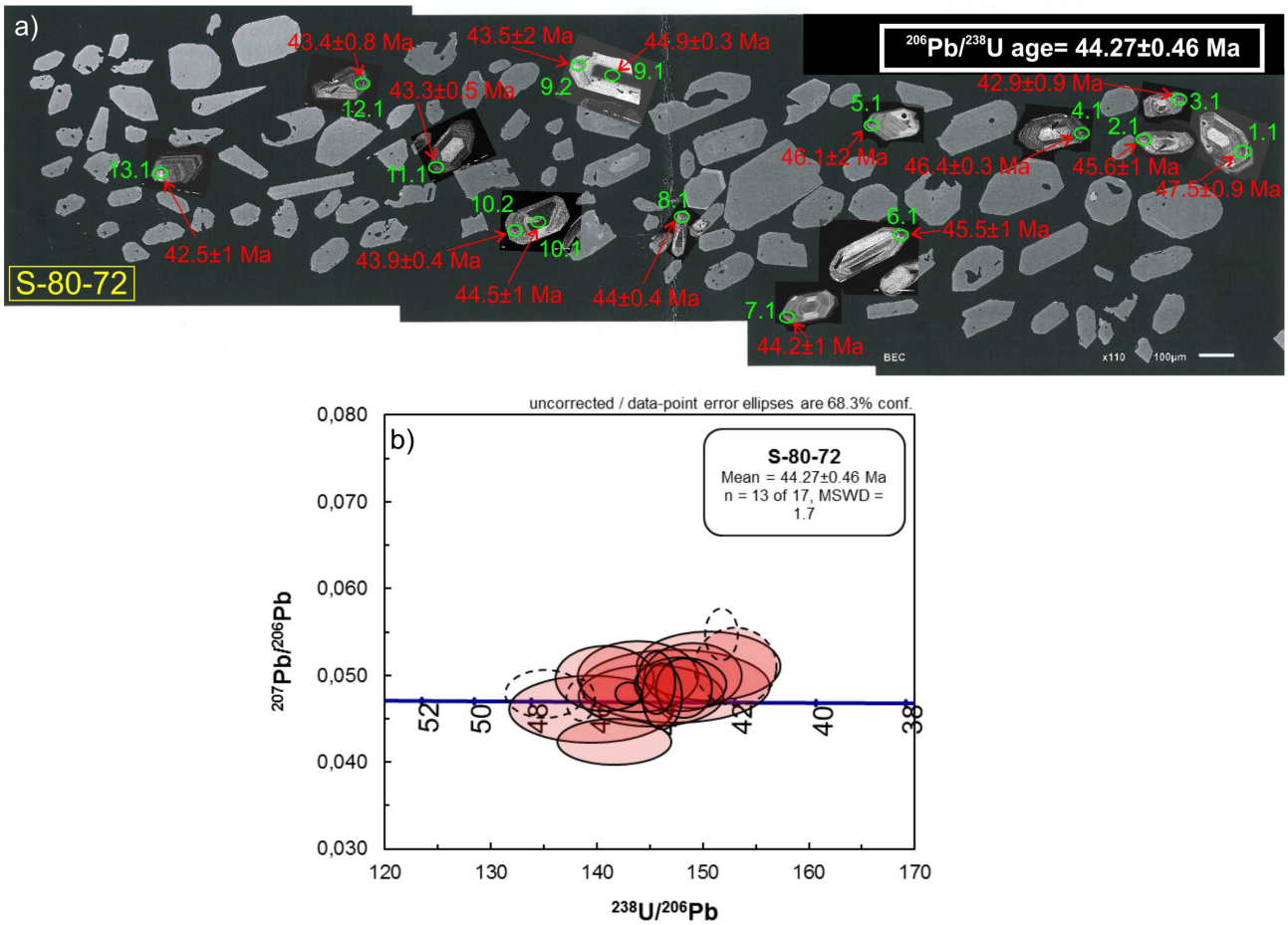

Figure 4. a) CL image and b) U-Pb Concordia diagram of zircons.

350 µm) and short to long prismatic with aspect ratios of approximately 2. Zircon grains possess pyramidal terminations and oscillatory zoning (Figure 4a). All features (pyramidal termination, oscillatory zoning etc.) show zircon growth from magma. Most analyses provided concordant age data. The mean $^{206}Pb/^{238}U$ age is 44.27±0.46 Ma (Table S1; Figure 4b). For the quartz porphyry, the Eocene age is defined using the U-Pb zircon dating and is commented as the magmatic settlement age. The U-Pb analyses of 17 zircons in the sample S-80-72 provided ages ranging from 47.5 to 41.8 Ma and a mean $^{206}Pb/^{238}U$ age of 44.27±0.46 Ma (Figure 4).

Mineral Chemistry of Tourmaline Formations

Electron microprobe analyses of tourmalines from the quartz porphyry in the Karadağ area were conducted (Table S2). Tourmaline crystals are mostly 50-200 µm in size (Figure 5). The Al_{tot} contents of tourmalines in the spotted and shear zones and among breccias are 5.38-6.50, 5.44-6.67, and 5.31-6.68, respectively (Table S2). The general formula of tourmaline is $XY_3Z_6(T_6O_{18})(BO_3)_3V_3W$, where X = Na, Ca, K, and vacancy; Y=$Fe^{2+/3+}$, Mg, Mn^{2+}, Li, Al, Cr, V^{3+}, Fe^{3+}, and Ti^{4+}; Z=Mg, Al, $Fe^{2+/3+}$, V^{3+}, and Cr^{3+}; T=Si, Al, and B^{3+}; B=B^{3+}; V=$(OH)^-$ and O^{2-}; W=$(OH)^-$, F^-, and O^{2-} (Henry et al., 2011; Bosi, 2018). The unit formula of tourmaline from the Karadağ area is the $^{X}(Na_{0.50\text{-}0.89}Ca_{0.002\text{-}0.25}K_{0.002\text{-}0.01}\square_{0\text{-}0.48})^{Y}(Al_{0\text{-}0.56}Fe^{2+}_{0.12\text{-}1.45}Mg_{1.10\text{-}2.33}Mn_{0\text{-}0.01}Ti_{0.01\text{-}0.21}Li^*_{0.05\text{-}0.40})_3{}^{Z}(Al_{5.38\text{-}6}Mg_{0\text{-}0.62})_6\ {}^{T}(Si_{5.79\text{-}6.1}Al_{0\text{-}0.21})_6\ O_{18}(BO_3)_3{}^{V}(OH)_3{}^{W}(O_{0\text{-}0.01}F_{0.01\text{-}0.35}OH_{0.64\text{-}0.99})$. The Al or Al-Mg substitution is noted to be occupied in the Z-site. Tourmaline crystalline shows concentric zoning related to Fe enrichment from the core to the rim (Table S2; Figure 6). Calculations of site occupancies show that tourmaline does not generally contain sufficient amount of Al to fill the Z-site (4.62-6.00 apfu in the spotted, 5.36-6.00 apfu in the shear zone, and 5.77-6.18 apfu among breccias; Table S2). Tourmaline shows a wide range of major element concentrations, especially Fe (0.12-1.45 apfu), Mg (1.10-2.33 apfu), and Al (5.38-6.18 apfu). Tourmaline is magnesian (Mg/

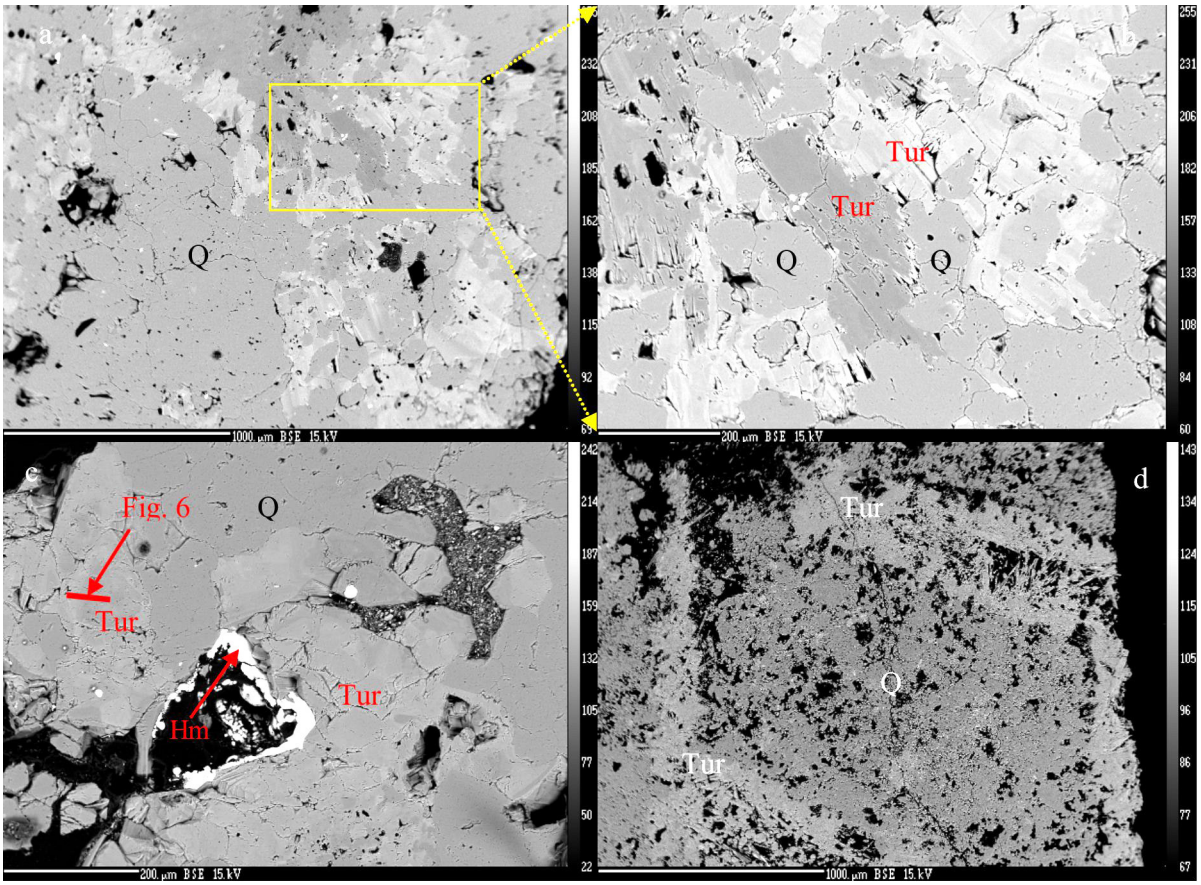

Figure 5. SEM images of tourmalines from Karadağ area showing a) and b) Tourmaline in the spotted (sample no: S-45), c) Tourmalines in the shear zone (sample no: S-72T) and d) tourmalines among breccias (sample no: S-80T). Q: Quartz, Tur: Tourmaline, Hm: Hematite.

(Mg+Fe)=0.58-0.92 in the spotted, 0.50-0.99 in the shear zone, and 0.41-0.90 among breccias). The Na/Na+Ca ratios of tourmaline vary from 0.88 to 1.0 in the spotted and from 0.7 to 1.0 in the shear zone and among breccias (Figure 7). The Na is the main cation in the X site (Table S2; Figure 7). The Ca in the structural formula is very low (0.01-0.25 apfu, atoms per formula unit). Moreover, tourmalines are poor in calcium [Ca/(Ca+Na) ratios 0.0-0.12 in the spotted, 0-0.29 in the shear zone, and 0.02-0.30 among breccias; Figure 8) with Na+K between 0.47 and 0.86 apfu (Na+K 0.67-0.86 in the spotted, 0.59-0.85 in the shear zone, and 0.47-0.85 among breccias). The F content in tourmalines is within the narrow range of 0.01 to 0.36 apfu. The calculated vacancies in the X-site vary from 0.07 to 0.35 in the spotted, from 0.10 to 0.41 in the shear zone, and from 0.07 to 0.49 among breccias (Table S2). The concentric zones, which are related to growth zoning, show chemical variations. The chemical zoning is Mg substitute for Fe and/or Al in the Y site and X-vacancy replacing Na in the X site (Table S2). Al and Mg display an apparent enrichment in the core and depletion in the rim. Tourmaline in Karadağ has decreased alkalinity in the R1+R2 versus R3 diagram (Figure 8c). Substitution of Al (R3) for R1+R2 in tourmaline is partly accommodated by alkali deficiency. As a result, all tourmalines belong to the alkali-group (Figure 8a). Tourmalines have low fluorine content (<1.0) and a wider range of the Fe/Fe+Mg ratio with 0.06-0.42 in the spotted, 0.01-0.50 in the shear zone, and 0.10-0.60 among breccias. All tourmalines, except few breccia tourmalines, can be classified between dravite and schorl, with the dravite component often prevailing over schorl; moreover, quartz porphyry samples are found between schorl and dravite fields (Figs 7, 8b). Karadağ tourmalines are mainly the Mg-rich end member (Figure 8d). Karadağ tourmalines have low Fe content and high Mg content. Al is high in all tourmaline.

The most common diagrams used for determining tourmaline types are the triangle diagrams of Al-Fe-Mg and Ca-Fe(tot)-Mg systems (Henry and Guidotti, 1985). The data drop largely in the host rock field defined as metapelites and metapsammites co-existing with an Al-saturating phase on the Al-Fe-Mg diagram (Figure

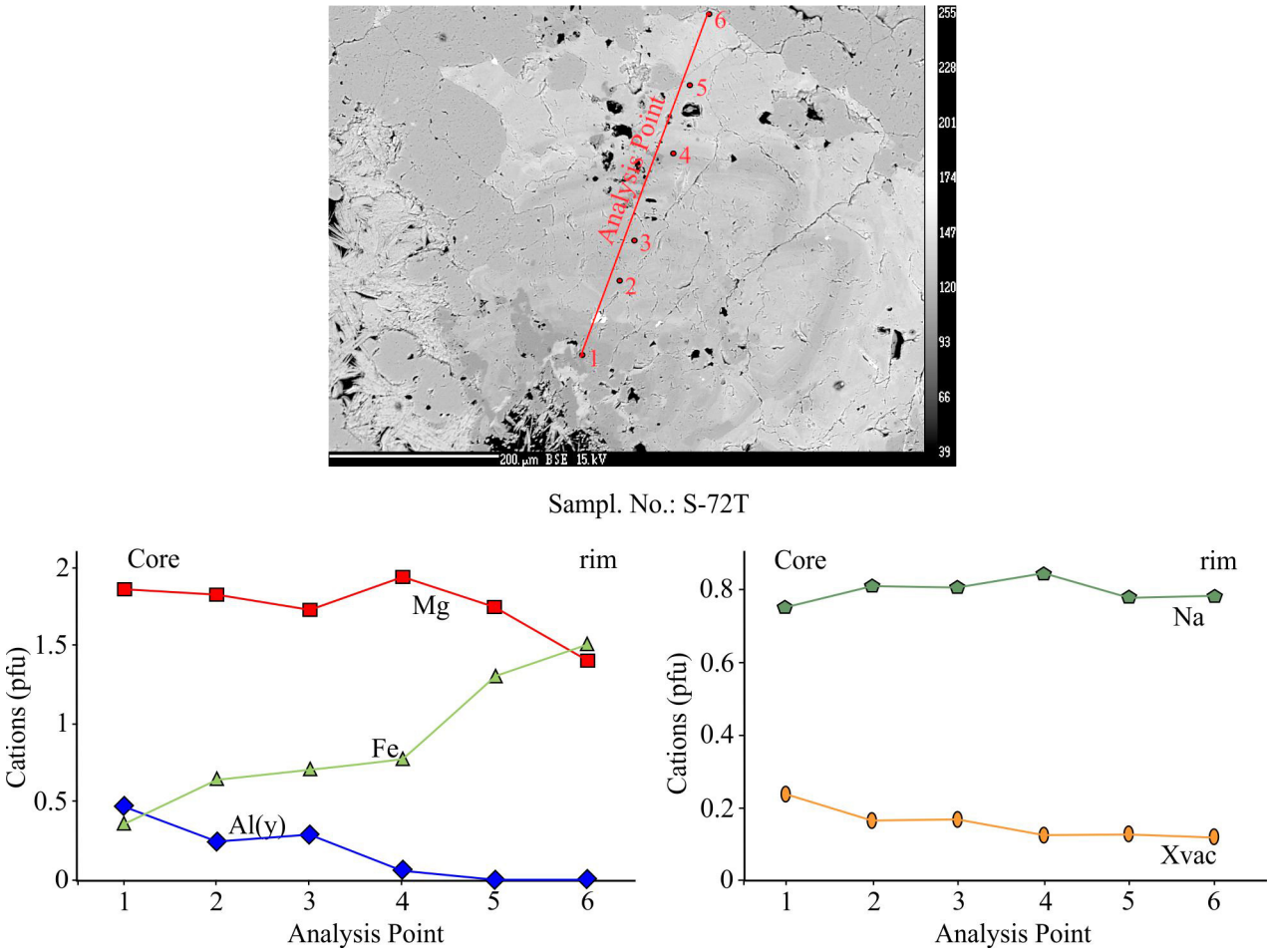

Figure 6. Zoning in the tourmaline. a) SEM image of zoning in the tourmaline, b) and c) Chemical zoning of tourmaline.

8e) and in the field defined as Ca-poor metapelites, metapsammites, and quartz-tourmaline rocks (Field 10) on the Ca-Fe(tot)-Mg diagram (Figure 8f).

Geothermometer of the Quartz Porphyry

Zircon and apatite saturation temperatures (Watson and Harrison, 1983; Hanchar and Watson, 2003; Miller et al., 2003) in the quartz porphyry were determined from the whole-rock geochemical data (Table 2). The abundance of Zr (99-449 ppm) and P_2O_5 (0.02-0.08 wt%) in the quartz porphyry samples was used to calculate zircon and apatite saturation temperatures. In the quartz porphyry, the zircon saturation temperatures change from 755 °C to 884 °C and the apatite saturation temperature is between 853 °C and 918 °C.

Geochemical Properties of Tourmaline Formations

The geochemistry of tourmaline and quartz porphyry showed differences (Table S3). The concentrations of K_2O (0.03-1.24 wt%), Rb (0.3-36 ppm), Sr (37.3-147.1 ppm), and Y (2.3-22.9 ppm) in tourmalines are lower than those of the quartz porphyry. Meanwhile, the concentrations of Al_2O3 (14.34-33.96 wt%), MgO (2.7-8.95 wt%), Fe_2O_{3t} (5.3-10.13 wt%), Ga (36.3-47.8 ppm), Ni (0.2-14.5 ppm), V (112-510 ppm), and Sn (7-58 ppm) in tourmaline are higher than those of the quartz porphyry. The FeO/(FeO+MgO) ratio for the tourmaline from the Karadağ area is between 0.11 and 0.72 (Figure 9a).

The REE contents in the tourmaline and quartz porphyry from the Karadağ area in Table S3 are normalized to the level of chondrite (Figure 9). The tourmaline and quartz porphyry have the same REE patterns, that is, slight depletion from light REE to heavy REE with $(La/Yb)_N$ ratios of 2.19 to 7.85 and 0.49 to 13.23, respectively. The REE pattern of the tourmaline generally resembles those of host quartz porphyry. The REE patterns of the tourmaline and quartz porphyry have negative Eu anomalies of 0.56-1.06 and 0.19-0.89, respectively.

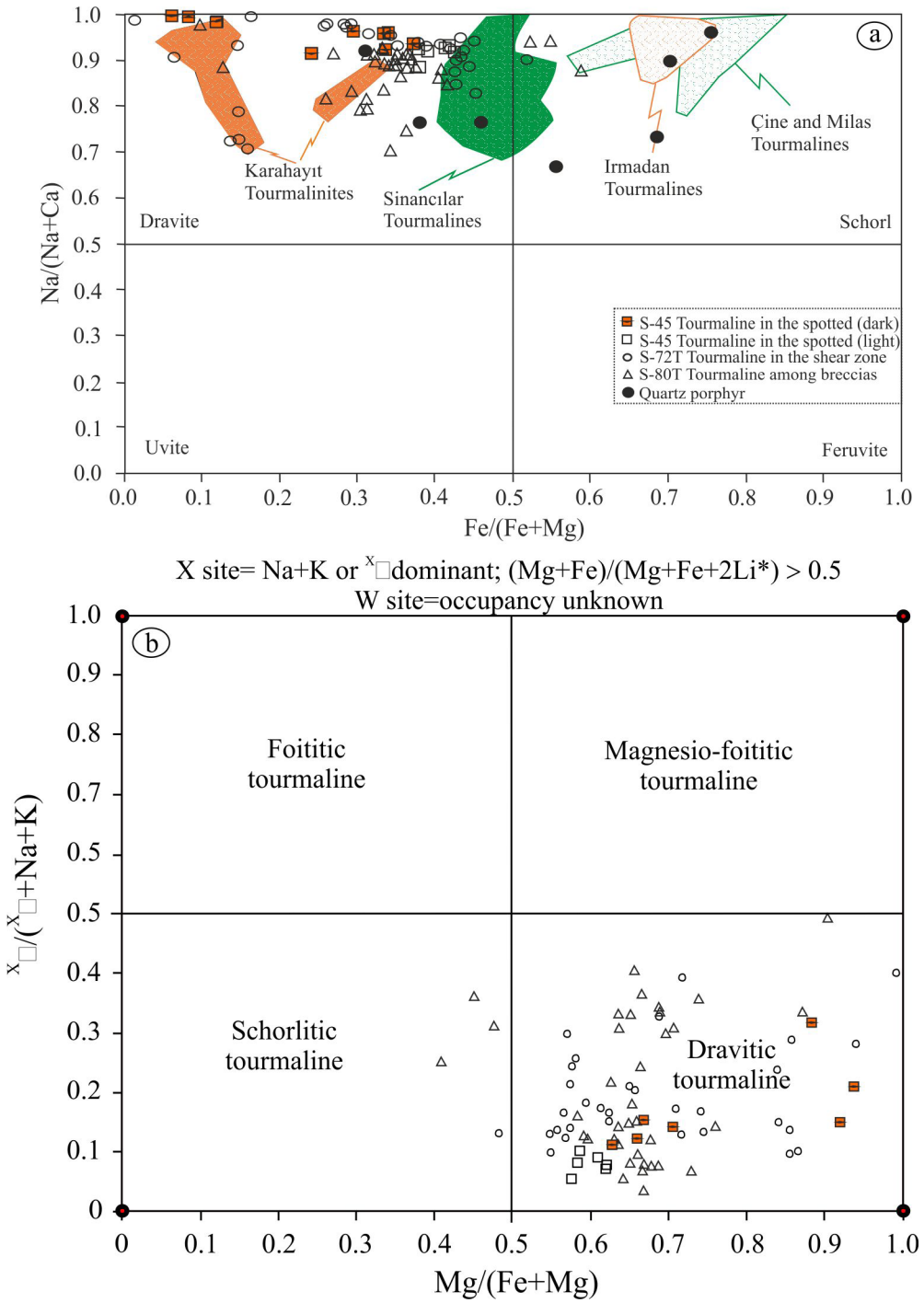

Figure 7. The tourmaline classification diagram [Sinancılar, Çine and Milas tourmalines from Oyman (2006); Karahayıt and Irmadan tourmalines from Yücel et al. (2015); Figure 7b modified from Henry et al. (2011)].

O and H isotopes

The $\delta^{18}O$ values obtained from the tourmaline and quartz porphyry from the Karadağ area and the δD values for the tourmaline are presented in Table 3. The $\delta^{18}O$ values of tourmalines vary from 5.7 to 8.5‰ and the dD values from -58 to -72‰. The $\delta^{18}O$ values of the quartz porphyry change from 9.2 to 9.3‰ (Figure 10). The $\delta^{18}O$ and δD values for tourmaline are plotted in Figure 9a. The tourmaline from Karadağ has an isotopic signature similar to those of primary magmatic water, igneous rock, and

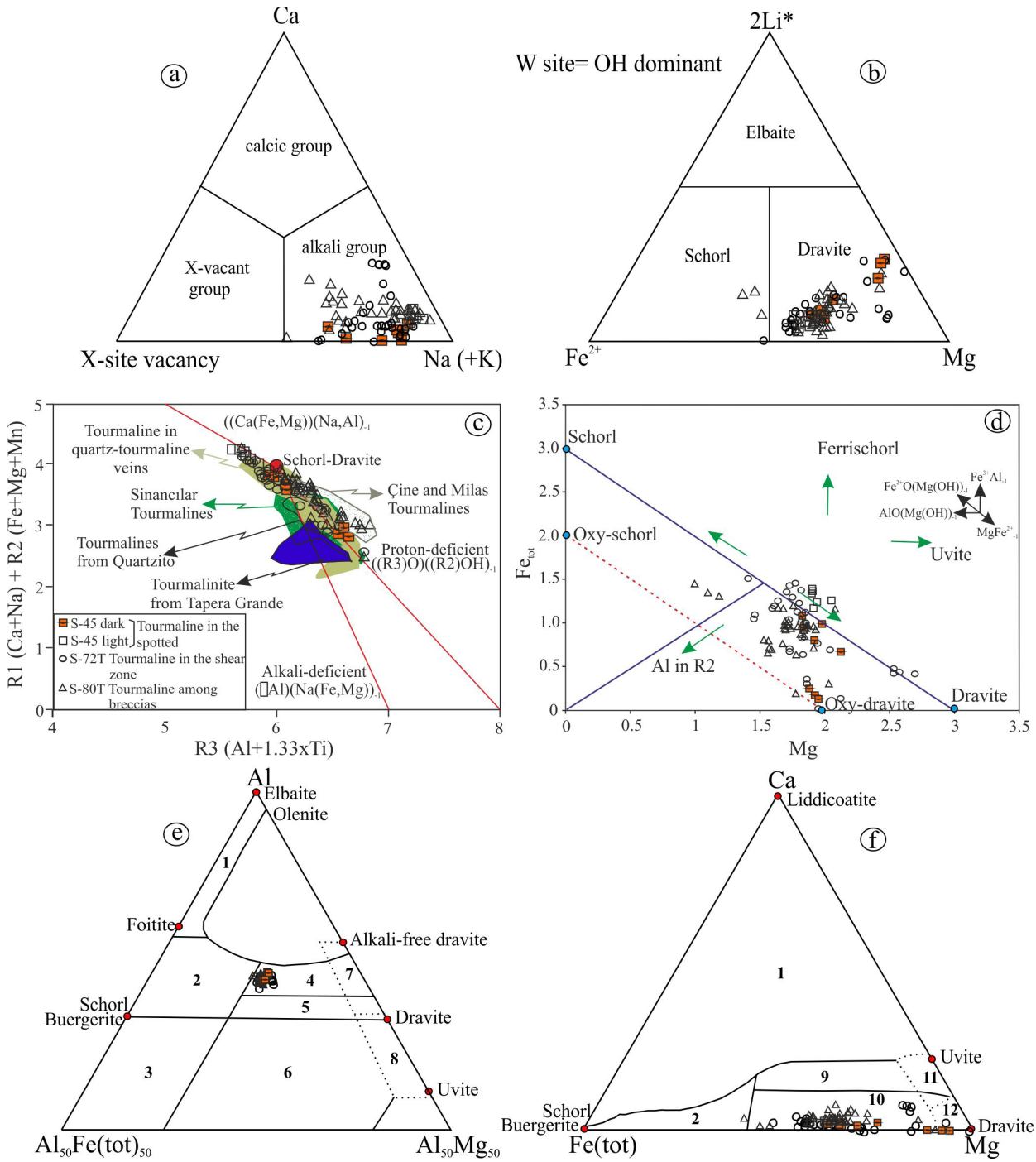

Figure 8. The ternary diagrams for the Karadağ Tourmaline compositions (a) based on X-site occupancies and b) classifying alkali-group tourmaline specie (Henry et al., 2011), c) The R3 vs R1+R2 diagram for Karadağ Tourmalines (Quartzito and Tapera Grande tourmalines from Garda et al. (2003); Sinancılar, Çine and Milas tourmalines from Oyman (2006); tourmaline in the quartz-tourmaline veins from Yavuz et al. (2008), d) The Mg vs Fe diagram showing variation of the Karadağ Tourmaline, e) Al-Fe(tot)-Mg ternary and d) Ca-Fe(tot)-Mg ternary diagram (after Henry and Guidotti, 1985) for tourmalines from Karadağ area diagram. (1) Li-rich granitoid pegmatites and aplites, (2) Li-poor granitoid pegmatites and aplites, (3) Fe^{3+}-rich-quartz-tourmaline rocks (hydrothermally altered granitic rocks), (4) Metapelites and metapsammites co-existing with Al-saturating phase, (5) Metapelites and metapsammites not co-existing with Al-saturating phase, (6) Fe-rich quartz-tourmaline rocks, calc-silicate rocks and metapelites, (7) Low Ca metaultramafics, metapelites, (8) Metacarbonates, and meta-pyroxenites, (9) Ca-rich metapelites, metapsammites, and calc-silicate rocks, (10) Ca-poor metapelites, metapsammites and quartz-tourmaline rocks, (11) Metacarbonates, and (12) Metaultramafics.

Table 2. Zircon and apatite crystallization temperatures from the quartz porphyry.

Sample no.	T °C (Zircon)	T °C (HW, apatite)
SG-2	884	847
SG-1	755	864
SG-3	830	869
S-5	808	853
SG	839	918
S-102	757	891

tourmaline in pegmatite. In addition, the isotopic values of the tourmaline are close to those of tourmalines in aplite-pegmatite dike. The values of $\delta^{18}O$ for tourmaline and quartz porphyry from the Karadağ area resemble the isotope fractionation between the tourmaline and quartz. According to Kotzer et al. (1993), the empirical oxygen isotope fractionation factor equation and the oxygen isotope thermometry calculations of the quartz and tourmaline pair at the Karadağ area indicated that these minerals were formed at 432 °C.

DISCUSSION

Tourmaline Chemical Substitution

Tourmalines in the Middle Eocene aged quartz porphyry are not common but occur locally in some quartz porphyry. The presence of breccias cemented by tourmaline suggests that tourmaline occurred after that the development of the quartz porphyry. The quartz porphyry without tourmaline crystals shows no brecciation. The presence of tourmaline among breccias suggests that boron along with water dominated in the exsolved fluid phase (Gaweda et al., 2013). The high contents of Ti (0.12-1.72 wt% in the spotted, 0.18-1.27 wt% in the shear zone, and 0.12-1.37 wt% among breccias) and Fe (0.96-9.92 wt% in the spotted, 0.18-10.72 wt% in the shear zone, and 2.36-10.22 wt% among breccias) were found in these tourmaline crystals. the result also indicated the lack of biotite in the quartz porphyry, mobilized by the boron-rich fluid (Gaweda et al., 2013). Local overpressure of boron-rich fluid in the quartz porphyry presumably can cause brecciation; meanwhile, precipitation of tourmaline in breccias could occur from probably heating and oxidizing fluid that exsolved from the cooling quartz porphyry magma.

All tourmalines from Karadağ are composed of dravite and belong to the alkali group (Figures 7, 8). Tourmaline species are described in suitable with the dominant valence rule. In a relevant site, the dominant ion of the dominant valence is utilized for the basis of nomenclature (Henry et al., 2011). The dominant anion at the W site of the tourmaline is OH, and the dominant species in that subgroup defines dravite (Figure 8b). In this study, the tourmaline in the quartz porphyry is characterized by poor Ca and rich Mg content. The tourmaline composition of hydrothermal origin is generally characterized by cation vacancies and poor Na content at the X site under relatively alkaline condition (Foit, 1989; Francis et al., 1999; Henry et al., 2002; Medaris et al., 2003). Tourmaline in country rocks possess higher Ca content than granitic and greisen tourmalines (London and Manning, 1995). The MgO content in tourmaline in the quartz porphyry is relatively high (6.90-7.68 wt% in the spotted, 5.96-11.01 wt% in the shear zone, and 3.98-9.06 wt% among breccias). Tourmaline is controlled by granitic rocks. The FeO/(FeO+MgO) content in tourmaline is proposed by Pirajno and Smithies (1992) as a proximity indicator. Tourmalines in granite may be considered as proximal to distal due to the distance from the granitic source (Rasekh et al., 2016). Tourmalines in granite have FeO/(FeO+MgO) values, ranging from 0.86 to 0.96, correspondingg to an endogranitic to proximal setting (Henry and Dutrow, 1996). Tourmalines in the Asarcık Granitoid is distal to proximal intermediate and have FeO/(FeO+MgO) values ranging from 0.41 to 0.80 (Figure 9a); meanwhile, the FeO/(FeO+MgO) values of tourmalines in the quartz tourmaline veins range from 0.23 to 0.95 and are considered as distal to endogranitic (Yavuz et al., 2008). As a result, the FeO/(FeO+MgO) values of tourmaline from the quartz porphyry in the study area change from 0.11 to 0.72 and represented as proximal to intermediate and distal (Figure 9a).

Substitution of Al (R3) versus R1+R2 in tourmalines indicates that they approach the ideal schorl-dravite composition (Foit and Rosenberg, 1977). Some tourmalines reflect partly alkali deficiency (Figure 8 c,d). All tourmalines fall in the host rock field that is described as Ca-poor metapelites, metapsammites, and quartz-tourmaline rocks (Figure 8f).

Trace Elements as Indication of Tourmaline Origin

Tourmalines in the study area have low Sr (37.3-147.1 ppm) and V (112-510 ppm) contents. Tourmaline concerned to granitic rocks typically has lower Sr and V contents than those concerned to metavolcanic or metapelitic rocks (Jiang et al., 2004; Galbraith et al., 2009; Hezel et al., 2011, Yavuz et al., 2011; Marks et al., 2013; Table 1; Figure 11). The V and Sr contents in tourmalines in the Karadağ area are consistent with those of magmatic and metamorphic tourmalines (Table 1; Figure 11).

The rare earth element patterns of q-porphyr and tourmalines in Karadağ were compared with those of tourmalines of the Karahayıt and Çine in the western Anatolia of the Turkey (Yücel-Öztürk et al., 2015). The samples in Karadağ show generally consistent trends

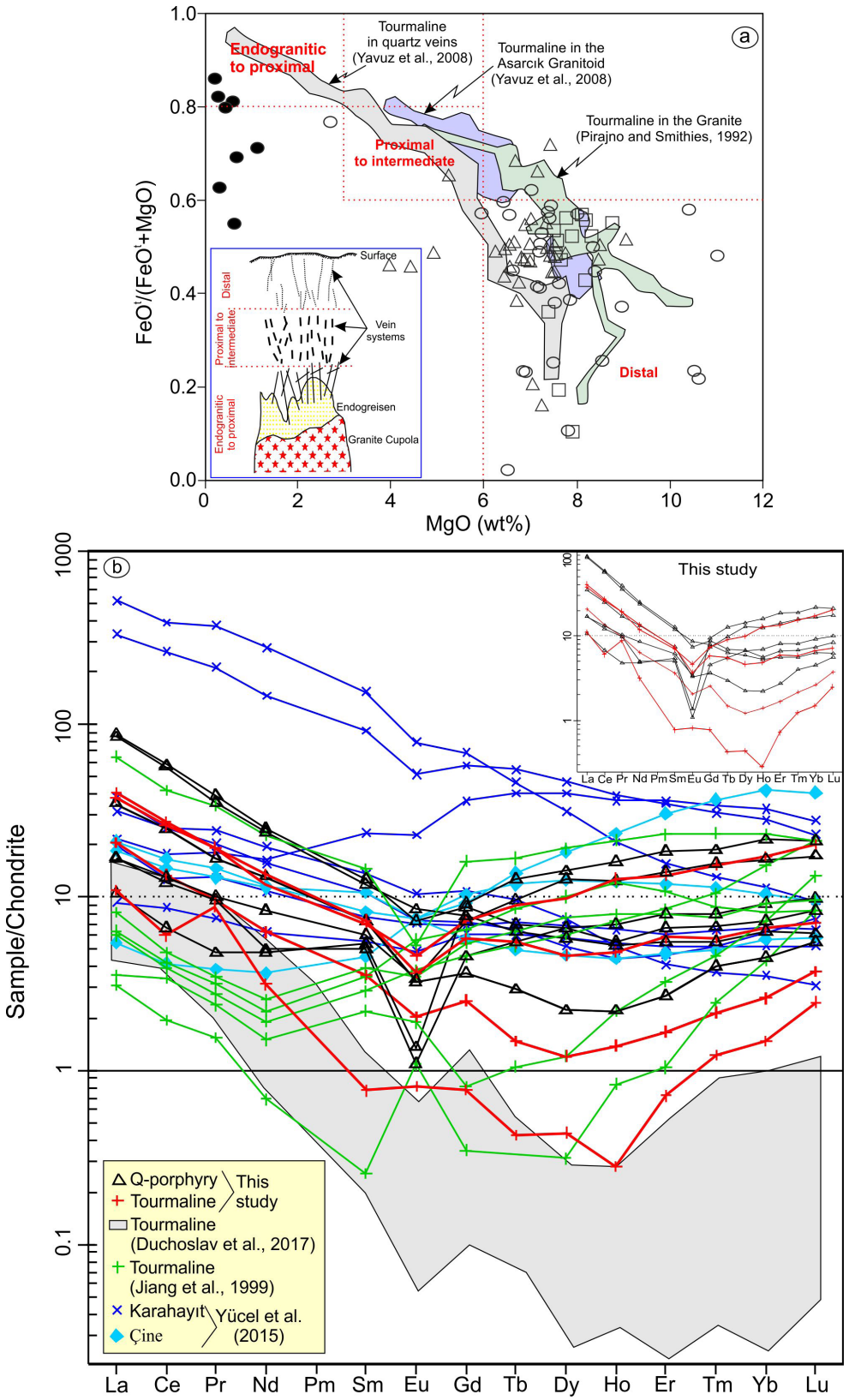

Figure 9. a) The $FeO^t/(FeO^t+MgO)$ vs MgO (diagram from Pirajno and Smithies, 1992; symbols are the same in Figure 8) and b) The chondrite-normalized diagram of tourmaline and quartz porphyry samples from the Karadağ area (chondrite data from Boynton, 1984).

Table 3. O and H isotopic data of tourmaline and quartz porphyry from the Karadağ area.

Sample	Mineral/Rock	$\delta^{18}O_{VSMOW}$ (‰)	δD_{VSMOW} (‰)	Calculated T °C[1]	References
S-45T	Radial tourmaline	6.8	-58		
S-72T	tourmaline with quartz in the shear zone	8.5	-69		
S-80T	Tourmaline breccia	5.7	-72	432	This study
S-80T1	Tourmaline	8.0	-66		
S-72	Quartz-porphyry	9.3	-		
S-80	Quartz-porphyry	9.2	-		
SRT-3-99	Tourmaline	12.0	-86		Garda et al. (2003)
FQ-112	Tourmaline	11.8	-102		
161	Tourmaline	10.30	-67		
156	Tourmaline	9.73	-73		Matthews et al. (2003)
8	Tourmaline	9.69	-62		

[1] Temperature calculated from Kotzer et al. (1993) for S-80 and S-80T samples of the quartz-tourmaline pairs.

except for two samples from Karahayıt. The REE patterns of tourmaline and quartz porphyry in Karadağ are similar to those of the Dachang (China) deposit (Jiang et al., 1999; Figure 8). Yücel-Öztürk et al. (2015) proposed that the metasomatic event occurred during the Late Palaeocene-Eocene partial subduction of the Menderes Massif. The samples of the tourmaline and quartz porphyry in Karadağ show richer LREEs than the tourmalines from the Dachang (China) deposit and the Cornubian batholith (SW England) and lower LREEs than the tourmalines in two samples of the Karahayıt. The tourmaline in the quartz porphyry has negative Eu anomaly, consistent with the fact that the quartz porphyry in Karadağ has negative Eu anomaly (Figure 9). The tourmaline in the Şebinkarahisar (Giresun, Turkey) is defined by negative Eu and positive Ce anomalies, reflecting the redox reactions during tourmaline formation from hydrothermal fluids (Yavuz et al., 2011). Marks et al. (2013) determined that the granite-connected pegmatitic tourmaline usually has negative Eu anomaly in the crust-normalized REE pattern, while the gneiss-related tourmaline has positive Eu-anomaly. Duchoslav et al. (2017) pointed out that Group I tourmaline from granite and greisen generally displays LREE-enriched patterns with negative Eu anomalies similar to those of the tourmaline in Karadağ (Figure 9).

Oxygen and Hydrogen Isotope of Tourmaline and Fluid Sources

The dD values of tourmalines varying from -58 to -72 ‰ in the study area coincide with the ranges reported by Kotzer et al. (1993) for pegmatitic tourmalines. The tourmaline from Karadağ has an isotopic signature similar to those of primary magmatic fluids and tourmaline in pegmatite (Jiang, 1998) as well as aplite-pegmatite dike (Matthews et al., 2003) and differs from the compositions that have resemblance to sediment waters, such as tourmalines from Tapera Grande and Quartzito (Garda et al., 2003; Figure 10). The oxygen isotope composition of the tourmaline drops in the "magmatic water" field (Figure 10). The calculated zircon saturation temperature range (755 °C-884 °C) for the quartz porphyry is typical of magmatic conditions. The oxygen isotope thermometry (432 °C) for tourmaline suggests that it occurred in post-magmatic setting in the quartz porphyry (Figure 10b). In addition, the oxygen isotope composition of the tourmaline in the quartz porphyry is similar to that of the tourmaline in pegmatite (Figure 10b).

CONCLUSIONS

Tourmaline in the Karadağ area belongs to the alkali group and is composed of dravite. The tourmaline in the quartz porphyry is characterized by poor Ca and rich Mg content. The tourmaline is controlled by contact metasomatic process and has high Mg and Al contents but low Ca content. The tourmaline shows chemical zoning being Mg substitute for Fe and/or Al in the Y site, and X-vacancy for Na in the X site from core to rim.

The tourmaline typically has lower Sr (37.3-147.1 ppm) and V (112-510 ppm) and is consistent with magmatic and metamorphic tourmalines. The REE pattern of tourmaline

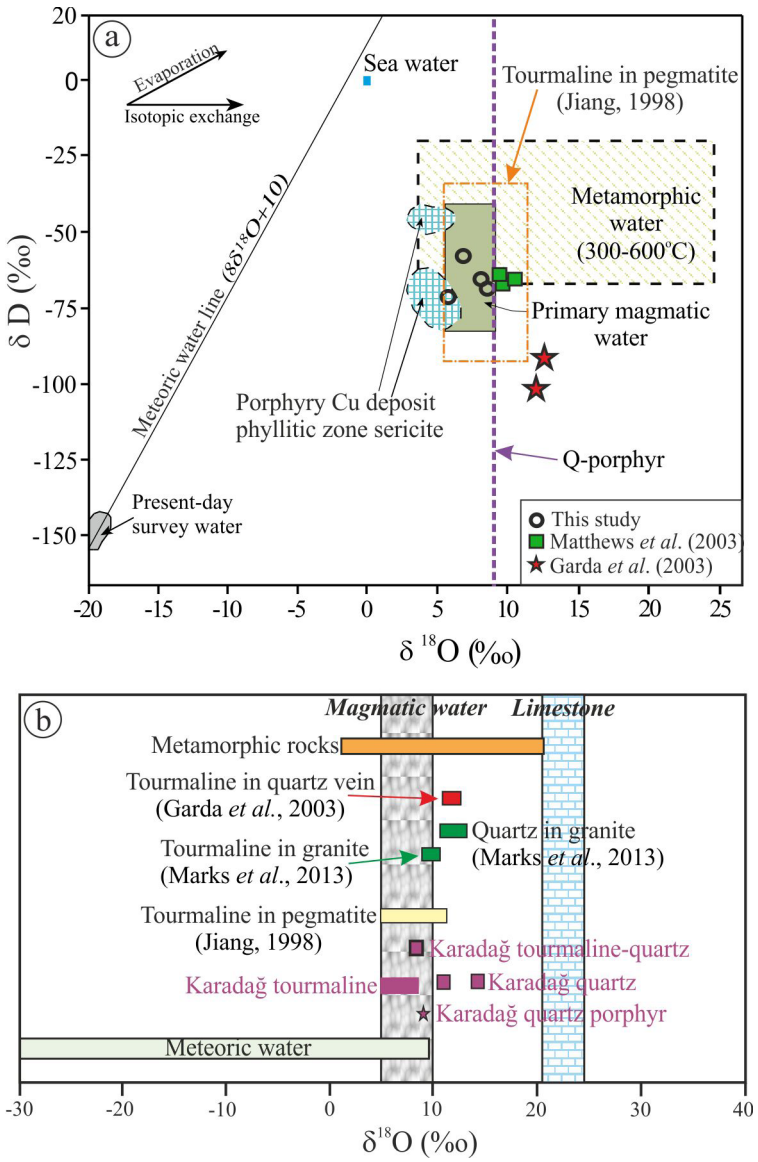

Figure 10. a) The isotopes properties of tourmalines and quartz porphyry from Karadağ area (NE Turkey) and b) $\delta^{18}O$ (‰) isotope variations of the tourmaline and quartz minerals (other data from Hoefs, 1987).

generally reflects those of the host quartz porphyry. The heavy REE contents of the tourmalines are lower than those of the host quartz porphyry. The tourmaline shows a negative Eu anomaly similar to the quartz porphyry.

Stable isotope values indicate magmatic source as fluid sources for the dravite type tourmaline, showing a (post-) magmatic origin at 432 °C. The $\delta^{18}O$ compositions for tourmaline and host quartz porphyry are similar, suggesting that fluid equilibration was formed during crystallization of the tourmaline. The variations in the chemical and isotopic compositions of the studied tourmalines support that magmatic formation is associated with the cooling of magmatic fluid and geochemical fluid-rock interactions.

ACKNOWLEDGEMENTS

Financial support for this study was provided by the 114Y099 numbered The Scientific and Technological Research Council of Turkey (TÜBİTAK). The author thanks to Prof. Dr. Keewok YI for The U-Pb zircon age analysis, Dr. Lynn HEIZLER for the electron microprobe analyses, and deceased Prof. Dr. Kurtis KYSER for oxygen and hydrogen isotopes analyses. İbrahim Akpınar, Tanju Aydurmuş and Cüneyt Doruk are thanked for their help during the fieldwork.

Conflicts of Interest

There is no conflict of interest with any author.

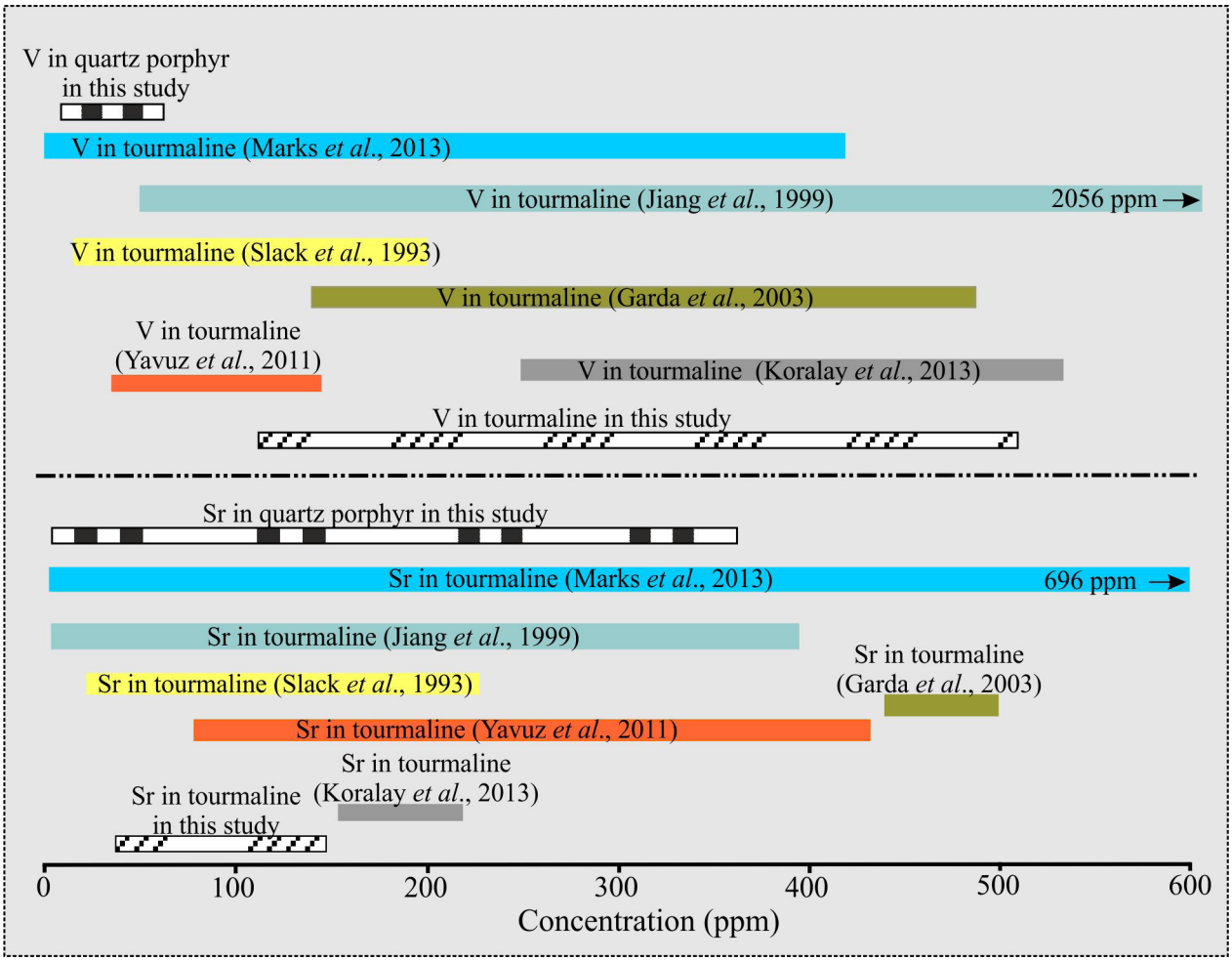

Figure 11. Concentrations of Sr and V elements in tourmaline and the quartz porphyr comparing with those of the other tourmalines.

REFERENCES

Akaryalı E., 2016, Geochemical, fluid inclusion and isotopic (O, H and S) constraints on the origin of Pb-Zn±Au vein-type mineralizations in the Eastern Pontides Orogenic Belt (NE Turkey). Ore Geology Reviews 74, 1-14.

Bosi F., 2018. Tourmaline crystal chemistry. American Mineralogist 103, 298-306.

Boztuğ D., Jonckheere R., Wagner G.A., Yegingil Z., 2004. Slow Senonian and fast Palaeocene-Early Eocene uplift of the granitoids in the Central Eastern Pontides, Turkey: apatite fission-track results. Tectonophysics 382, 213-228.

Boynton W.V., 1984, Cosmochemistry of the Rare Earth Elements; Meteorite Studies. In: Henderson P. (Ed.), Rare Earth Element Geochemistry, Elsevier Science Publishing Company, Amsterdam, pp. 63-114.

Deb M., Tiwary A., Palmer M.R., 1997. Tourmaline in Proterozoic massive sulfide deposits from Rajasthan, India. Mineralium Deposita 32, 94-99.

Galbraith C.G., Clarke D.B., Trumbull R.B., Wiedenbeck, M., 2009. Assessment of tourmaline compositions as an indicator of emerald mineralization at the Tsa da Glisza Prospect, Yukon Territory, Canada. Economic Geology 104, 713-731.

Garda G.M., Beljavskis P., Juliani C., Silva D., 2003. Geochemistry of tourmalines associated with iron formation and quartz veins of the Morro da Pedra Preta Formation, Serra do Itaberaba Group (São Paulo, Brazil). Anais da Academia Brasileira de Ciências 75, 209-234.

Gaweda A., Müller A., Stein H., Kadziolko-Gawel M., Mikulski S., 2013. Age and origin of the tourmaline-rich hydraulic breccias in the Tatra Granite, Western Carpathians. Journal of Geosciences 58, 133-148.

Francis C.A., Dyar M.D., Williams M.L., Hughes J.M., 1999. The occurrence and crystal structure of foitite from a tungsten-bearing vein at Copper Mountain, Taos County, New Mexico. Canadian Mineralogy 37, 1431-1438.

Foit F.F. and Rosenberg P.E., 1977. Coupled substitutions in the tourmaline group. Contributions to Mineralogy and Petrology 62, 109-127.

Foit F.F. Jr., 1989. Crystal chemistry of alkali-deficient schorl and tourmaline structural relationships. American Mineralogist 74, 422-431.

Griffin W.L., Slack J.F., Ramsden A.R., Win T.T., Ryan C.G., 1996. Trace elements in tourmaline from massive sulfide deposits and tourmalinites: Geochemical controls and exploration applications. Economic Geology 91, 657-675

Hanchar J.M. and Watson E.B., 2003. Zircon saturation thermometry. In: Hanchar, J.M., and Hoskin, P.W.O. (Ed.), Zircon, Review in Mineralogy and Geochemistry 53. Mineralogical Society of America, Geochemical Society of America, pp. 89-112.

Hellingwerf R.H., Gatedal K., Gallagher V., Baker J.H., 1994. Tourmaline in the central Swedish ore district. Mineralium Deposita 29, 189-205.

Henry D.J. and Dutrow B.L., 1996. Metamorphic tourmaline and its petrologic applications. In: Grew, E.S., and Anovitz, L.M. (Eds.). Boron: Mineralogy, Petrology and Geochemistry, Rev. Mineral. 33, 503-557.

Henry D.J. and Guidotti C.V., 1985. Tourmaline as a petrogenetic indicator mineral: an example from the staurolite-grade metapelites of NW Maine. American Mineralogist 70, 1-15.

Henry D.J., Novák M., Hawthorne F.C., Ertl A., Dutrow B.I., Uher P., Pezzotta F., 2011. Nomenclature of the tourmaline-supergroup minerals. American Mineralogist 96, 895-913.

Henry D.J., Dutrow B.L., Selverstone J., 2002. Compositional asymmetry in replacement tourmaline - an example from the Tauern Window, Eastern Alps. Geol. Mater. Res. 4, 1-18.

Hezel D.C., Kalt A., Marschall H.R., Ludwig T., Meyer H.-P., 2011. Major-element and Li, Be compositional evolution of tourmaline in an S-type granite-pegmatite system and its country rocks: an example from Ikaria, Aegean Sea, Greece. The Canadian Mineralogist 49, 321-340.

Hoefs J., 1987. Stable isotope geochemistry, 3rd ed. Springer, Berlin-Heidelberg-New York 241 p.

Jiang S.Y., 1998. Stable and radiogenic isotope studies of tourmaline: An overview. Journal of the Czech Geological Society 43, 1-2, 75-90.

Jiang S.-Y., Han F., Shen J.-Z., Palmer M.R., 1999. Chemical and Rb-Sr, Sm-Nd isotopic systematics of tourmaline from the Dachang Sn-polymetallic ore deposit, Guangxi Province, P.R. China. Chemical Geology 157, 49-67.

Jiang S.Y., Palmer M.R., Li Y.-H., Xue C.-J., 1995. Chemical compositions of tourmaline in the Yindongzi-Tongmugou Pb-Zn deposits, Qinling, China: implications for hydrothermal ore-forming processes. Mineralium Deposita 30, 225-234.

Jiang S.Y., Palmer M.R., Peng Q.M., Yang J.H., 1997. Chemical and stable isotopic compositions of Proterozoic metamorphosed evaporates and associated tourmalines from Houxianyu borate deposit, eastern Liaoning, China. Chemical Geology 135, 189-211.

Jiang S.Y., Palmer M.R., Slack J.F., Shaw D.R., 1998. Paragenesis and chemistry of multistage tourmaline formation in the Sullivan Pb-Zn-Ag deposit, British Columbia. Economic Geology 93, 47-67.

Jiang S.-Y., Yu J.-M., Lu J.-J., 2004. Trace and rare-earth element geochemistry in tourmaline and cassiterite from the Yunlog tin deposit, Yunnan, China: implication for migmatite-hydrothermal fluid evolution and ore genesis. Chemical Geology 209, 193-213.

Jolliff B.L., Papike J.J., Shearer C.K., 1987. Fractionation trends in mica and tourmaline as indicators of pegmatite internal evolution: Bob Ingersoll pegmatite. Black Hills, South Dakota. Geochimica et Cosmochimica Acta 51, 519-534.

Kaygusuz A., Arslan M., Siebel W., Sipahi F., İlbeyli N., Temizel İ., 2014. LA-ICP MS zircon dating and whole-rock Sr-Nd-Pb-O isotope geochemistry of the Camiboğazı pluton, Eastern Pontides, NE Turkey: Petrogenesis and tectonic implications of arc-related I-type magmatism. Lithos 192-195, 271-290.

King R.W. and Kerrich R.W., 1989. Strontium isotope compositions of tourmaline from Iode gold deposits of the Archean Abitibi greenstone belt (Ontario-Quebec, Canada): Implication for source reservoirs. Chemical Geology 79, 225-240.

King R.W., Kerrich R.W., Daddar R., 1988. REE distributions in tourmaline: an INAA technique involving pretreatment by B volatilization. American Mineralogist 73, 424-431.

Koralay T., Kadıoğlu Y.K., Jiang S.-Y., 2013. Determination of Tourmaline Composition in Pegmatite From Buldan, Denizli (Western Anatolia, Turkey) Using XRD, XRF, and Confocal Raman Spectroscopy. Spectroscopy Letters 46, 499-506.

Kotzer T.G., Kyser T.K., King R.W., Kerrich R., 1993. An empirical oxygen- and hydrogen isotope geothermometer for quartz-tourmaline and tourmaline-water. Geochimica et Cosmochimica Acta 57, 3421-3426.

London D. and Manning D.A.C., 1995. Chemical variation and significance of tourmaline from Southwest England. Economic Geology 90, 495-519.

Ludwig K.R., 2008. User's manual for Isoplot 3.6: a geochronological toolkit for Microsoft Excel. Berkeley Geochronology Center Special Publication, 4, 77 p.

Lynch G. and Ortega J., 1997. Hydrothermal alteration and tourmaline-albite equilibria at the Coxheat porphyry Cu-Mo-Au deposit, Nova Scotia. Canadian Mineralogist 35, 79-94.

Marks M.A.W., Marschall H.R., Schühle P., Guth A., Wenzel T., Jacob D.E., Barth M., Markl G., 2013. Trace element systematics of tourmaline in pegmatitic and hydrothermal systems from the Variscan Schwarzwald (Germany): The importance of major element composition, sector zoning, and fluid or melt composition. Chemical Geology 344, 73-90.

Matthews A., Putlitz B., Hamiel Y., Hervig R.L., 2003. Volatile transport during the crystallization of anatectic melts: Oxygen, boron and hydrogen stable isotope study on the metamorphic complex of Naxos, Greece. Geochimica et Cosmochimica Acta 67, 3145-3163.

Medaris L.G., Fournelle J.H., Henry D.J., 2003. Tourmaline-

Bearıng Quartz Veins in the Baraboo Quartzite, Wisconsin: Occurrence and Significance of Foitite And "Oxy-Foitite". The Canadian Mineralogist 41, 749-758.

Miller C.F., Meschter McDowell S., Mapes R.W., 2003. Hot and cold granites? Implications of zircon saturation temperatures and preservation of inheritance. Geology 31, 529-532.

Mlynarczyk M.S.J. and Williams-Jones A.E., 2006. Zoned tourmaline associated with cassiterite: implications for fluid evolution and tin mineralization in the San Rafael Sn-Cu deposit, southeastern Peru. Canadian Mineralogist 44, 347-365.

Neiva A.M.R., Silva M.M.V.G., Gomes M.E.P., 2007. Crystal chemistry of tourmaline from Variscan granites, associated tin-tungsten- and gold deposits, and associated metamorphic and metasomatic rocks from northern Portugal. Neues Jahrbuch für Mineralogie - Abhandlungen 184, 45-76.

Okay A.I. and Tüysüz O., 1999. Tethyan sutures of northern Turkey. In: Durand, B., Jolivet, L., Horváth, F., and Séranne, M. (Eds.), The Mediterranean Basins: Tertiary Extension within the Alpine Orogen, Special Publications, Geological Society London, 156, pp. 475-515.

Okay A.I., Şahintürk Ö., Yakar H., 1997. Stratigraphy and tectonics of the Pulur (Bayburt) region in the Eastern Pontides. Mineral Research Expolaration Bulletin 119, 1-24.

Oyman T., 2006. Crystal Chemistry of the tourmalines from granites and pegmatites in metamorphic rocks of the Aegean Region. DEÜ Mühendislik Fakültesi Fen ve Mühendislik Dergisi 8, 47-65 (in Turkish with English abstract).

Özdoğan K., 1992. Karadağ (Torul-Gümüşhane) ve yakın çevresinin jeolojisi-mineralojisi-petrografisi ve maden zuhurlarının jenetik incelenmesi. Ph.D. Thesis, Selçuk Üniversitesi, Fen Bilimleri Enstitüsü, Konya, Turkey.

Paces J.B. and Miller Jr.J.D., 1993. Precise U-Pb ages of Duluth Complex and related mafic intrusions, Northeastern Minnesota: geochronological insights to physical, petrogenic, paleomagnetic, and tectonomagmatic processes associated with the 1.1 Ga midcontinent rift system. Journal of Geophysical Research 98, 13997-14013.

Palmer M.R., 1991. The boron isotope systematics of hydrothermal fluids and tourmaline: A synthesis. Chemical Geology 94, 111-121.

Pirajno F. and Smithies R.H., 1992. The FeO/(FeO+MgO) ratio of tourmaline: a useful indicator of spatial variations in granite-related hydrothermal mineral deposits. Journal of Geochemical Exploration 42, 371-381.

Rasekh P., Mirmohammadi M., Esfahani M.M., 2016. Origin and Chemical Characteristics of Tourmaline in Kahang Porphyry Copper Deposit, NE Isfahan, Central Province of Iran. Workshops the 34th National and 2th International Geosciences Congress, February 22-24, Tehran, Iran, 10 p.

Sipahi F., 2011, Formation of skarns at Gümüşhane (Northeastern Turkey). Neues Jahrbuch für Mineralogie-Abhandlungen, 188, 169-190.

Sipahi F., Akpınar İ., Saydam Eker Ç., Kaygusuz A., Vural A., Yılmaz M., 2017. Formation of the Eğrikar (Gümüşhane) Fe-Cu skarn type mineralization in NE Turkey: U-Pb zircon age, lithogeochemistry, mineral chemistry, fluid inclusion, and O-H-C-S isotopic compositions. Journal of Geochemical Exploration 182, Part A, 32-52.

Sipahi F., Kaygusuz A., Saydam Eker Ç., Vural A., 2018b. Investigation of geology, geochemistry and geochronology of skarn mineralizations developed with granitoids (Gümüşhane, NE Turkey). Tubitak 1001 Project, No: 114Y099, Ankara, Turkey, 298 p.

Sipahi F., Kaygusuz A., Saydam Eker Ç., Vural A., Akpınar İ., 2018a. Late Cretaceous arc igneous activity: The Eğrikar Monzogranite Example. International Geology Review 60, 382-400.

Sipahi F. and Sadıklar M.B., 2010. The alteration mineralogy and mass change of the Zigana (Gümüşhane) volcanics of NE Turkey. Geological Bulletin of Turkey 53, 122-155.

Skewes M.A., Holmgren C., Stern C.R., 2003. The Donoso copper-rich, tourmaline bearing breccia pipe in central Chile: petrologic, fluid inclusion and stable isotope evidence for an origin from magmatic fluids. Mineralium Deposita 38, 2-21.

Slack J.F., 1996. Tourmaline associations with hydrothermal ore deposits. Rev. Mineral. 33, 559-643.

Slack J.F., Palmer M.R., Stevens B.P.J., Barnes R.G., 1993. Origin and significance of tourmaline-rich rocks in the Broken Hill District, Australia. Economic Geology 88, 505-541.

Stacey J.S. and Kramers J.D., 1975. Approximation of terrestrial lead isotope evolution by a two-stage model. Earth and Planetary Science Letters 26, 207-221.

Topuz G., Altherr R., Schwarz W.H., Siebel W., Satır M., Dokuz A., 2005. Postcollisional plutonism with adakite-like signatures: the Eocene Saraycık granodiorite (Eastern Pontides, Turkey). Contributions to Mineralogy and Petrology 150, 441-455.

Watson E.B. and Harrison T.M., 1983. Zircon Saturation Revisited Temperature and Composition Effects in a Variety of Crustal Magma Types. Earth and Planetary Science Letters 64, 295-304.

Williams I.S. and Hergt J.M., 2000. U-Pb dating of Tasmanian dolerites: a cautionary tale of SHRIMP analysis of high-U zircon. In: Beyond 2000: New Frontier, In: Woodhead J.D., Hergt J.M. and Noble W.P. (Ed.), Isotope Geoscience, Lorne, 2000, Abstracts and Proceedings, pp. 185-188.

Yavuz F., Fuchs Y., Karakaya N., Karakaya M.Ç., 2008. Chemical composition of tourmaline from the Asarcık Pb-Zn-Cu±U deposit, Şebinkarahisar, Turkey. Mineralogy and Petrology 94, 195-208.

Yavuz F., Jiang S.-Y, Karakaya N. Çelik Karakaya M., Yavuz R., 2011. Trace-element, rare-earth element and boron isotopic compositions of tourmaline from a vein-type Pb-Zn-Cu±U deposit, NE Turkey. International Geology Review 53, 1-24.

Yılmaz S. and Boztuğ D., 1996. Space and time relations of three

plutonic phases in the Eastern Pontides, Turkey. International Geology Review 38, 935-956.

Yücel-Öztürk Y., Helvacı C., Palmer M.R., Ersoy E.Y., Freslon N., 2015. Origin and significance of tourmalinites and tourmaline-bearing rocks of Menderes Massif, western Anatolia, Turkey. Lithos 218-219, 22-36.